JOURNAL OF MATERIALS SCIENCE 32 (1997) 3443–3450

Transmission electron microscopy of a transformation toughened white cast iron

S. K. HANN, J. D. GATES
Department of Mining and Metallurgical Engineering, The University of Queensland, Queensland 4072, Australia

J. V. BEE
Department of Mechanical Engineering, University of Adelaide, South Australia 5005, Australia

Transmission electron microscopy has been used to study the microstructure of an experimental white cast iron, in which a combination of modified alloy composition and unconventional heat treatment has resulted in a fracture toughness of 40 MPa $m^{-1/2}$. Microstructural features of the alloy that contribute to the toughness improvement and hence distinguish it from conventional white irons have been investigated. In the as-cast condition the dendrites are fully austenitic and the eutectic consists of M_7C_3 carbides and martensite. During heat treatment at 1130 °C the austenite is partially destabilized by precipitation of chromium-rich M_7C_3 carbides. This results in a dendritic microconstituent consisting of bulk retained austenite and secondary carbides which are sheathed with martensite. The martensite sheaths, which contain interlath films of retained austenite, are irregular in shape with some laths extending into the bulk retained austenite. Emphasis has been placed on the morphology, distribution, and stability of the retained austenite and its transformation products in the dendrites. The implications of these findings on the transformation toughening mechanism in this alloy are discussed.

1. Introduction

White cast irons are commonly used in service situations requiring a high degree of resistance to abrasive wear. The application of these materials to a wider range of service conditions tends to be limited by their inherently low fracture toughness. Manipulation of both composition and heat treatment have been explored by various authors [1–4] with the view to improving the fracture toughness.

The dendritic micro-constituent of these alloys is principally austenitic in the as-cast condition, due to a high degree of supersaturation of carbon and alloying elements in the austenite [5, 6] which depresses the onset temperature of the martensite transformation (the martensite start temperature), M_s to well below room temperature. If a harder martensitic or mixed austenite/martensite structure is desired (as is usually the case), heat treatment is required to "destabilize" the austenite. The heat treatment provides the thermal activation necessary for precipitation of chromium rich secondary carbides, resulting in reduction of the carbon and chromium levels in solution and an increase in the M_s temperature, leading to partial or substantial transformation to martensite during subsequent cooling. The amount of retained austenite remaining after destabilization increases with increasing destabilization temperature [5].

A popular white cast iron alloy composition is 2.8C–20Cr–2Mo–1Cu (ASTM A532-93a class II type D, AS 2027-1985 grade CrMoCu2021). In the as-cast and tempered (200 °C) condition, these alloys give typical plane-strain fracture toughness levels of 23–30* MPa $m^{1/2}$ [7, 8]. After the conventional heat treatment (destabilize 1000 °C, stress relieve 200 °C) they give 22–29* MPa $m^{1/2}$ [7, 8].

A modified white cast iron has been developed with a fracture toughness K_{Ic}, of 27–31 MPa $m^{1/2}$ in the as-cast condition and 38–42 MPa $m^{1/2}$ in the heat treated condition [8]. This very substantial increase in the fracture toughness was achieved by a combination of modifications, principally a reduction in carbon content (from 2.8 to 1.9%) and a high temperature heat treatment (1130 °C). It has been demonstrated that the increase in toughness is largely due to a strain induced martensite (SIM) transformation toughening mechanism [9]. Strong evidence has also been

* Ranges of measured values for the 2.8C alloy under the experimental conditions used in the author's laboratory are 24–27 MPa $m^{1/2}$ in the as-cast condition and 24–28 MPa $m^{1/2}$ after conventional heat treatment [7]. Full ranges of values from the literature are 20–32 MPa $m^{1/2}$ as-cast and 18–32 MPa $m^{1/2}$ heat treated [8].

advanced [7] that the secondary carbides play a key role in the fracture, probably by increasing the frequency with which cracks leave the eutectic constituent and enter the dendrites. Finally, it has been shown that spheroidization of eutectic carbides is *not* occurring to any significant extent at these heat treatment temperatures [7].

The resolution limit of optical microscopy has made it difficult to characterize in detail the microstructural features believed to control the fracture of these alloys, namely the martensite, retained austenite and secondary carbides. In particular, in alloys known to contain a mixture of martensite and retained austenite, it is difficult to discern the precise locations of these phases within the microstructure, because (a) they may be interspersed on a fine scale, (b) the differential etching characteristics of the austenite and martensite can be ambiguous, and (c) fine dispersions of secondary carbides complicate the structure and can sometimes be mistaken for martensite laths, especially since the preferentially etched boundaries of the carbides may be more easily seen than the carbides themselves.

Transmission electron microscopy (TEM) provides the image resolution and analytical tools needed to resolve these ambiguities, and has been performed by a few authors [10–17] on conventional (full carbon) white cast irons. One disadvantage of TEM studies has been the difficulty of preparing thin foil specimens. With conventional electrolytic polishing techniques it is difficult to obtain uniform thinning of eutectic carbides and matrix phases, while heavy thinning using ion milling can introduce artefacts.

This paper reports a first TEM study of the microstructure of the modified white cast iron alloy. Both the as-cast and heat treated conditions are examined. Particular attention is paid to the distribution and morphology of retained austenite and its transformation products in the dendrites, since the SIM mechanism is dependent upon these.

2. Experimental procedure

Alloys were cast using the investment casting process from a 150 kg melt in an open induction furnace at a commercial foundry. The composition of the reduced carbon white iron studied is shown in Table I. The composition of a conventional iron (also examined in the author's laboratory) is also included for comparison. Specimens were cast as bars of dimensions $190 \times 42 \times 21$ mm, suitable for three-point bend fracture toughness testing.

All heat treatments were performed on whole fracture toughness bars. The heat treatment consisted of a 4 h destabilization treatment at 1130 °C, carried out in a heat resisting steel (253MA) box packed with a mixture of sand and coke. The coke/sand mixture has been previously shown to prevent significant decarburization but without the danger of carburization. After the destabilization period, the box was removed from the furnace and allowed to cool in still air to room temperature. Specimens were then subcritically treated (tempered) at 200 °C for 2 h and air cooled to room temperature.

Specimens for optical metallography were etched in acid ferric chloride. Specimens for TEM were prepared using a two stage electropolishing and ion milling process with particular emphasis being placed on avoiding either deformation induced or thermally induced transformation during thinning. Slices of 0.5–0.8 mm in thickness were cut from a bulk specimen using a water-cooled abrasive saw at a slow feed rate to avoid specimen heating. These were then mounted on a grinding block using double sided adhesive tape. Specimens were ground to approximately 200 μm, with the final grinding stage being performed on both sides of the specimen on 600 grit SiC paper. Discs were then individually cut using an ultrasonic cutter and a SiC cutting suspension. These were then further ground to a thickness of 80–100 μm on 1000 grit Si-C paper.

During electrolytic polishing trials it was found that specimens tended to be preferentially etched around the perimeter of the disc. In order to avoid this effect, discs were dimple ground to a thickness of approximately 40 μm in the central region. Electropolishing and subsequent ion milling were conducted at room temperature, eschewing the usual refrigeration, in order to avoid transformation of retained austenite at the M_s temperature (previously measured by differential scanning calorimetry to be -30 °C [9]). Electropolishing was carried out using a Tenupol-3 twin-jet polishing machine using a 10% perchloric-acetic acid electrolyte at 20V resulting in a specimen current of approximately 0.1A. Using a trial and error process it was possible to remove the specimen from the polishing cell just prior to perforation. Foils were then ion milled to perforation for 13 h at 4 kV at an angle of 10° and finally for 6 h at 5 kV at an angle of 5°.

The foils were examined using a Jeol 4000 FX ATEM and a Philips CM 200 TEM, operating at 400 and 200 kV respectively.

3. Results and discussion

3.1. As-cast condition

The general as-cast microstructure is shown by optical microscopy in Fig. 1.

Fig. 2(a) shows an example of the eutectic carbides and the eutectic iron "matrix" phase. Using selected

TABLE I Composition (wt %) of reduced-carbon alloy studied

Alloy	C	Cr	Mo	Ni	Si	Mn	Cu	V	S	P
Reduced C	1.9	18	1.9	1.6	1.2	1.1	1.0	0.4	0.01	0.02
Conventional	2.8	19	2.6	1.1	0.7	1.0	1.0	0.4	0.01	0.02

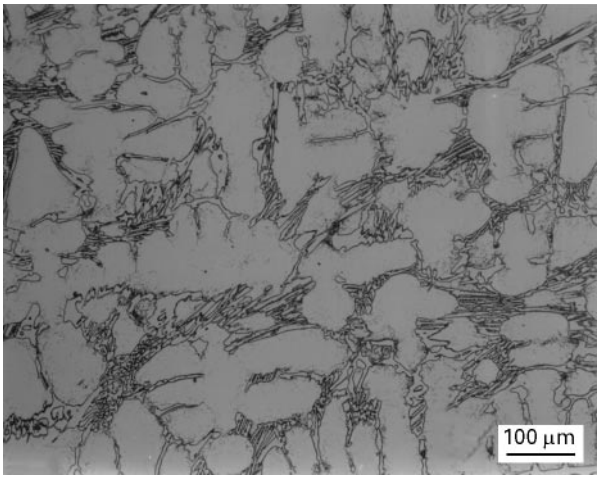

Figure 1 Optical micrograph of the as-cast microstructure.

area electron diffraction (SAED) the eutectic carbides were identified as M_7C_3. The eutectic matrix was identified as martensite.

In Fig. 2a, contrast from stacking faults can be seen within the eutectic carbides. Streaking on the electron diffraction patterns was observed along the directions of type $[1\,0\,\bar{1}\,0]$ and $[1\,1\,\bar{2}\,0]$. The observation of streaking along the directions of type $[1\,0\,\bar{1}\,0]$ (Fig. 2b) is in agreement with the common observation [12, 18] that stacking faults lie on the $\{1\,0\,\bar{1}\,0\}_{M_7C_3}$ planes. The observation of streaking along the directions of type $[1\,1\,\bar{2}\,0]$ (Fig. 2c) has not been frequently documented prior to this, but it is in agreement with the work of Morniroli *et al.* [19] who showed that for Fe_7C_3 carbides the structure contains ordered microdomains separated by $\{1\,1\,\bar{2}\,0\}$ defects.

Also in common with previous investigations of white cast irons [13] is the observation of apparently hollow rods of eutectic M_7C_3 carbide filled with "cores" of matrix constituent. Fig. 3a shows a eutectic carbide that has been sectioned transverse to its longitudinal growth direction. Contrast arises both from stacking faults parallel to the edges of the hexagonal rods and from the grain boundaries (or sub-grain boundaries [13]) that occur within them. Pearce [13] noted that these formations were consistent with the growth mechanism proposed by Ohide and Ohira [20] which suggests that M_7C_3 carbides form as hexagonal shells that grow inwards leaving a melt cavity of matrix at the centre. Fig. 3a shows that the reduced-carbon alloy contains a similar structure and the diffraction pattern from the resultant eutectic matrix "core", Fig. 3b, demonstrates that it is martensitic.

The dendrites appear to be fully austenitic with no evidence of transformation to martensite. There was little evidence of the deformation structures in the austenitic dendrites that have been observed by Powell and Bee [16] for a conventional high-carbon white iron.

3.2. Heat-treated condition

After destabilization, the eutectic microconstituent appears unchanged from that in the as-cast alloy. Only the dendritic microconstituent appears to have changed, the most obvious change being the presence of precipitated carbides.

Fig. 4 is an optical micrograph of the heat treated alloy showing the distribution of the rod shaped precipitated carbides in the dendritic microconstituent. These were identified by SAED as M_7C_3 chromium rich carbides. No $M_{23}C_6$ carbides were found. Pearce [14] found that the secondary carbides in a 15Cr–3.1C iron were M_7C_3 while those in a 30Cr–2.4C iron were $M_{23}C_6$. The observation for our reduced-carbon 18Cr iron corresponds to the former of Pearce's alloys, despite the fact that its Cr/C ratio is closer to that of the latter. In an alloy with 18Cr–3.1C–1.1Mo, Powell and Bee [16] primarily found M_7C_3 carbides after a conventional heat treatment, but in the early stages of heat treatment found only $M_{23}C_6$. The kinetic favourability of this non-equilibrium phase was explained [16] in terms of the good lattice matching between $M_{23}C_6$ and the austenite from which it precipitates. It is interesting once again to note that $M_{23}C_6$ was not observed in the reduced-carbon alloy, despite what might be presumed to be greater favourability of $M_{23}C_6$ in alloys with higher Cr/C ratios.

Fig. 5 is a TEM micrograph of a faceted M_7C_3 precipitated carbide that has been sectioned transverse to its [0 0 0 1] zone axis. The micrograph was obtained by tilting the specimen slightly off the pole revealing contrast from three sets of faults similar to those observed in the eutectic carbides. This observation differs from that of Pearce [13] who found that, while eutectic M_7C_3 carbides contained up to three visible sets of faults, secondary M_7C_3 carbides characteristically displayed only one set of faults corresponding to $\{1\,0\,\bar{1}\,0\}$ planes.

Fig. 6 shows the martensitic transformation "sheaths" (arrowed) which typically surround both the eutectic and precipitated carbides. These sheath structures appear consistent with the observations of Powell and Bee [16] who have linked their presence with a local rise in the M_s temperature caused by the depletion of carbon and chromium. In the case of eutectic carbides, Powell and Bee presented evidence to suggest that this depletion is as a consequence of solid-state growth of the carbides during heat treatment, not a solidification effect, and in the case of the secondary carbides solid state growth is of course the only possibility. Fig. 7(a and b) are a bright field and centred dark field pair illustrating that martensite laths extend from the transformed sheaths into the remaining "bulk" austenite. The dark field image (Fig. 7b) shows contrast from internal twins along the length of the lath. Fig. 8(a and b) are a bright field and centred dark field pair of a transformation sheath adjacent to a eutectic carbide. The dark field micrograph shows bright contrast from the presence of interlath retained austenite. Interlath retained austenite is a common observation in alloyed martensitic steels [21, 22].

As expected from optical microscopy and X-ray diffraction (XRD), TEM shows that the dendrites predominantly consist of retained austenite. Quantitative XRD indicated an overall austenite to martensite ratio of 0.85 [9]. Coupled with the observation that the

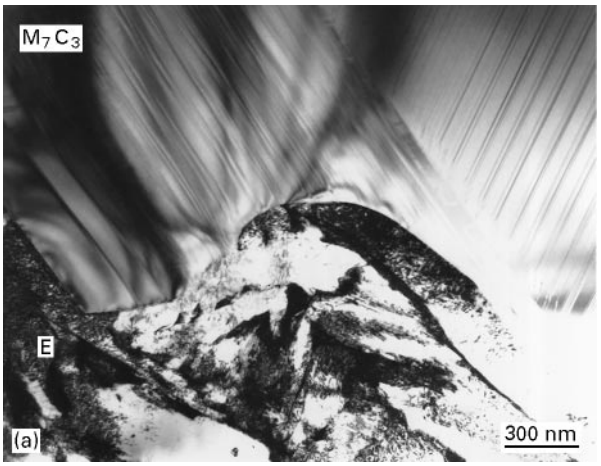

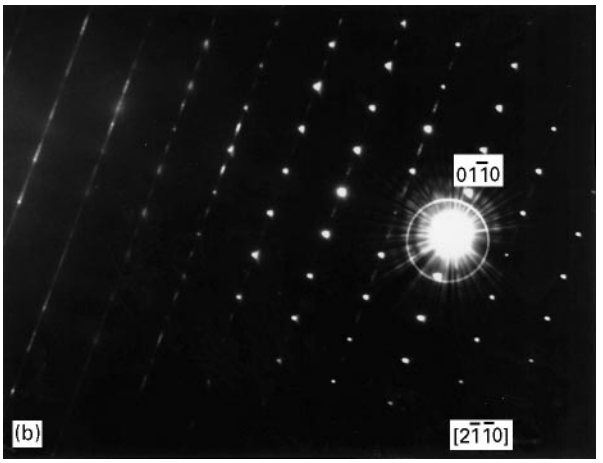

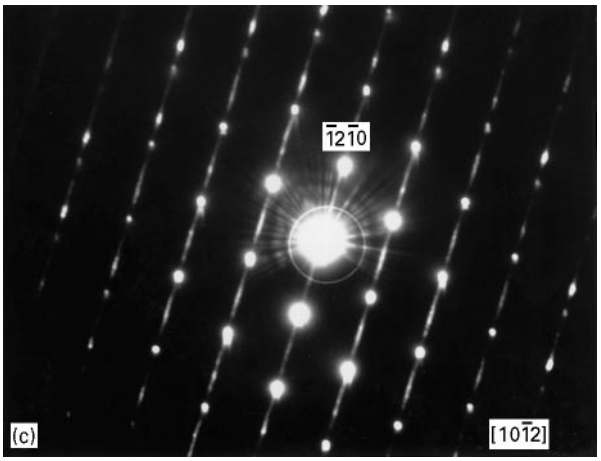

Figure 2 (a) TEM micrograph of the eutectic M_7C_3 carbides and eutectic matrix (E). Streaking contrast in carbides from defects on $\{1\,0\,\bar{1}\,0\}$ and $\{1\,1\,\bar{2}\,0\}$ planes. (b) and (c) Diffraction patterns from faulted M_7C_3 carbides. Fig. 2b showing contrast from streaking in directions of type $[1\,0\,\bar{1}\,0]$ and Fig. 2c showing contrast from streaking in directions of type $[1\,1\,\bar{2}\,0]$.

eutectic matrix is martensitic, this indicates that the sheaths of martensite around the secondary carbides constitute only a small volume fraction of the dendritic microstructure.

This "bulk" retained austenite, shown in Fig. 9, is heavily faulted. These severe faulting structures were observed in the heat treated alloy only and not in the as-cast state.

In the faulted retained austenite, contrast arises from stacking faults on the close packed $\{1\,1\,1\}_\gamma$ planes. This was confirmed by dark field images containing contrast arising from streaking on diffraction patterns taken from a number of similarly faulted regions in the foil, an example of which is shown in Fig. 10. Brooks *et al.* [23] showed, in their TEM *in-situ* cooling and *in-situ* straining experiments on stainless steels, that stacking fault structures of this type can be formed in retained austenite both by mechanical deformation and by cooling to just below the M_s temperature (giving partial transformation). They observed that these defects were closely associated with the martensite transformation, since they occurred at temperatures very close to M_s and since subsequent martensite nucleation occurred at these sites.

A question then arises as to what causes these deformation structures in the retained austenite. It could be that they are caused by the undercooling *per se*, being a change which occurs in retained austenite

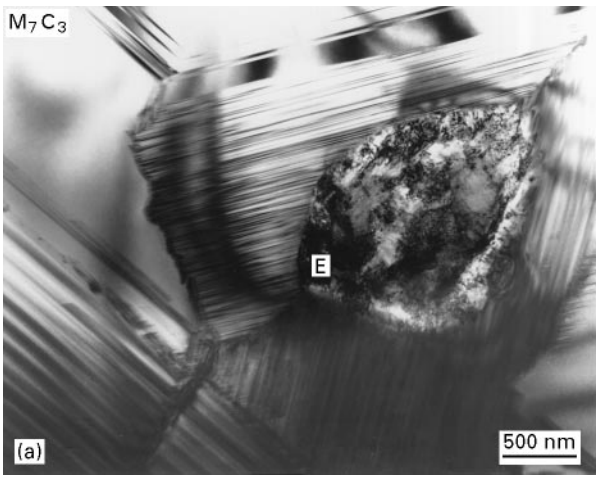

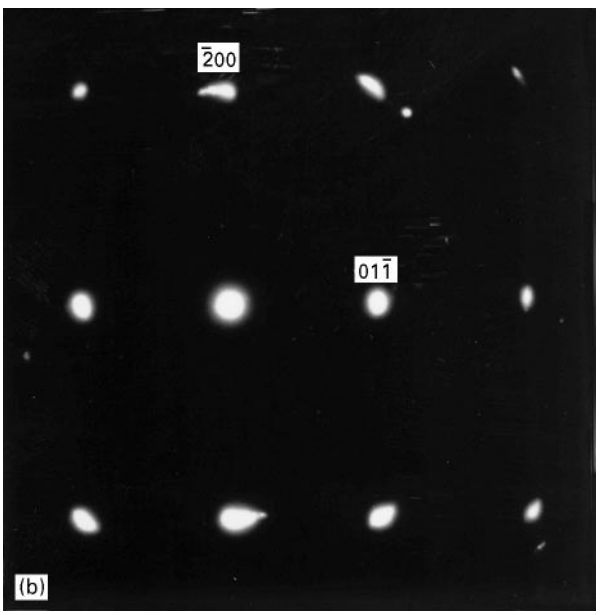

Figure 3 Bright field image and diffraction pattern from eutectic M_7C_3 carbide with martensitic matrix "core" (E). Carbide shows contrast from stacking faults and internal grain boundaries. Diffraction pattern is taken from matrix "core" and is indexed B = z = [0 1 1] body centred cubic (b c c).

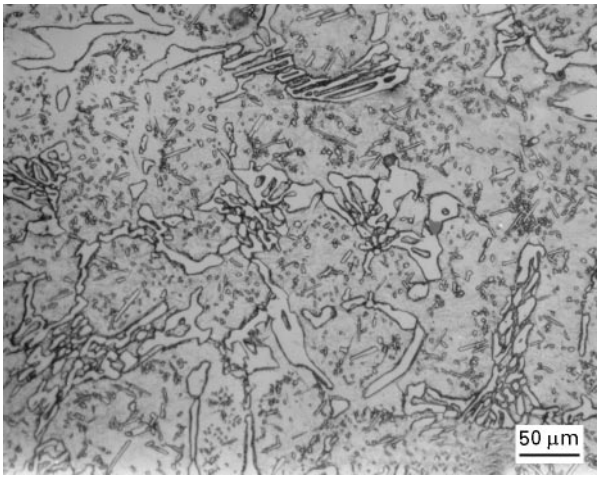

Figure 4 Optical micrograph of the heat treated alloy showing the distribution of the rod shaped precipitated carbides in the dendritic microconstituent.

Figure 5 Bright field image of a precipitated M_7C_3 carbide. Contrast is visible from three sets of stacking faults (arrowed) occurring on the $\{1\,0\,\bar{1}\,0\}$ planes.

immediately above M_s as a precursor to martensite transformation. Alternatively, it may be that they are only formed at temperatures below M_s, in the retained austenite affected by the volume expansion associated with the martensitic transformation that has already occurred. In the present work the deformation could come from the martensitic transformation around the secondary carbides.

This question could potentially be resolved if the precise M_s of the bulk retained austenite was known, but this is difficult to determine because dilatometers that can cool continuously from destabilization temperatures of 1130 °C to sub-ambient temperatures are not common. Some regions of the microstructure, such as the solute-depleted zones surrounding the secondary carbides, have M_s temperatures above room temperature, but it is uncertain whether the bulk retained austenite would have an M_s just below this or whether the chemical inhomogeneity allows much lower values. Differential scanning calorimetry (DSC) has measured the M_s temperature of the retained

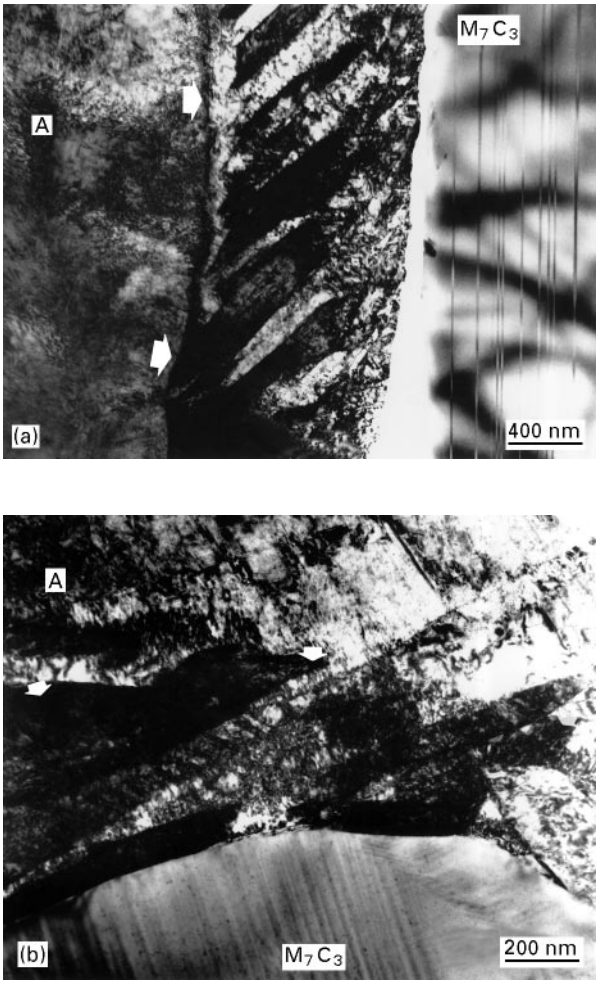

Figure 6 (a) and (b) Bright field images from the heat treated alloy showing M_7C_3 carbides with contrast from the transformation "sheaths" (arrowed) that typically surround them. These separate the carbide phase from the retained austenite (A).

austenite to be approximately − 30 °C [9], i.e., about 50° below room temperature. However, it is possible that the M_s of this constituent on cooling from the destabilization treatment was originally higher than this but that, upon the temperature arrest at room temperature, it was depressed by the phenomenon of "thermal stabilization" [24]. Thermal stabilization of austenite due to interruption of cooling between M_s and M_f (the martensite finish temperature) has been observed in many ferrous systems. In the current work DSC experiments have shown that when transformation is interrupted at sub-ambient temperatures the M_s measured upon subsequent cooling is some 50° lower than the arrest temperature. Thus, it cannot yet be determined whether the faulting structures are due to transformation-associated deformation or to cooling to just above M_s.

In the context of the above argument about the possible effect of the temperature arrest, it should be noted that in service the material has experienced this arrest. Thus it would be fallacious to regard the original M_s of this constituent (prior to the arrest) as the "true" M_s of the material. The M_s of the heat treated iron has been measured to be − 30 °C, and this evidently places it within the reach of strain-inducement of transformation to martensite and the consequent transformation toughening effect.

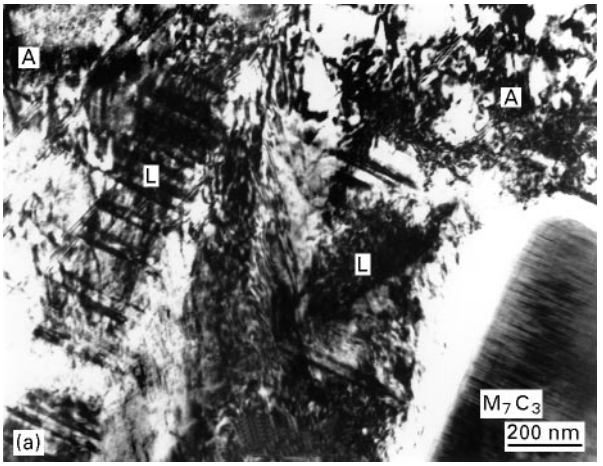

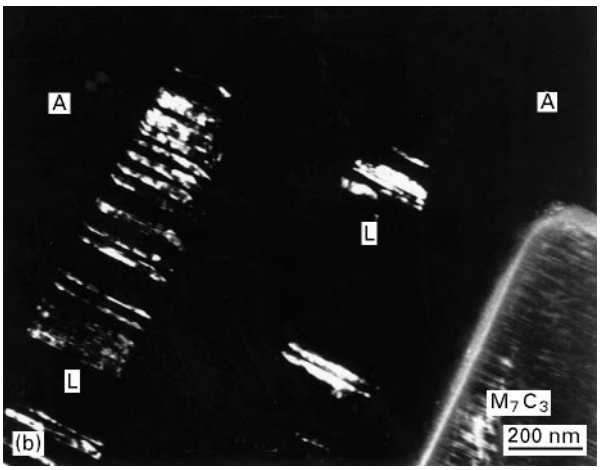

Figure 7 Bright field (a) and centred dark field (b) pair showing the presence of martensite laths (L) that extend into the remaining "bulk" austenite (A) from regions adjacent to the transformation "sheaths". Contrast is visible from internal twinning along the length of the lath.

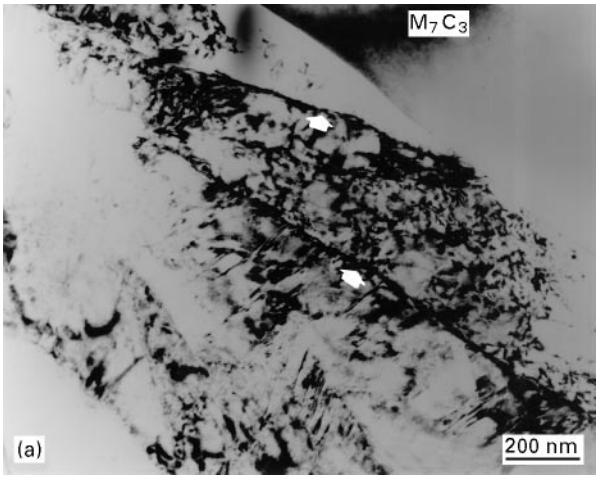

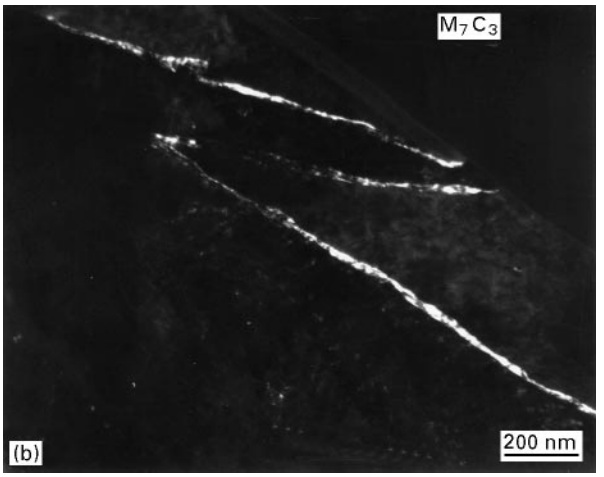

Figure 8 Bright field (a) and centred dark field (b) pair showing the presence of retained austenite (A) between the martensite laths that comprise the transformation "sheath" surrounding a eutectic M_7C_3 carbide.

There is some evidence of other decomposition products occurring in the regions adjacent to the carbides. Fig. 11 shows dark field contrast from a region in the vicinity of a eutectic carbide that has a morphology similar to that identified by Ricks *et al.* [25] as Widmanstätten ferrite sawteeth in an Fe–Cr–Ni alloy. It is possible that these structures may occur as a consequence of local variation in alloy composition.

3.3. Implications for fracture behaviour

It has been shown [9] that in the heat treated condition fracture is accompanied by a broad zone (about 400 μm or three dendrite-arm widths on either side of the crack) of strain-induced transformation of metastable retained austenite to martensite. In the as-cast condition, by contrast, the austenite is too stable to transform. It has been demonstrated that this SIM can explain most of the increase in fracture toughness in the heat treated alloy.

It has also been shown [7] that the secondary carbides play an important role in the fracture behaviour of the heat treated alloy, their presence correlating with an increase in the proportion of the crack passing through dendrites. The areal fraction of secondary carbides on the fracture surface is very much greater than that on polished sections, and increases with increasing destabilization temperature despite the concurrent decrease in the volume fraction of secondary carbides in the bulk due to the increased solubility [7]. From this it is concluded that the secondary carbides are instrumental in increasing the frequency with which cracks leave the eutectic constituent and enter the dendrites. It has been proposed [7] that the increment in fracture toughness due to this "crack diversion" is a function of two factors, namely (i) the frequency with which cracks enter the dendrites and (ii) the energy absorbed during cracking through the dendrites. When the dendritic matrix is substantially martensitic, as is the case with conventional heat treatments, little extra energy is absorbed. Consequently, the fracture toughness of conventionally treated irons is similar to that of as-cast (fully austenitic) irons, where the crack remains almost exclusively in the eutectic constituent [7].

The fact that as-cast austenitic irons do not have dramatically superior fracture toughness to martensitic irons indicates that an austenite matrix, although ductile, will only absorb significant crack energy if the crack enters the dendrites or at least causes the dendrites to be deformed. This evidently does not

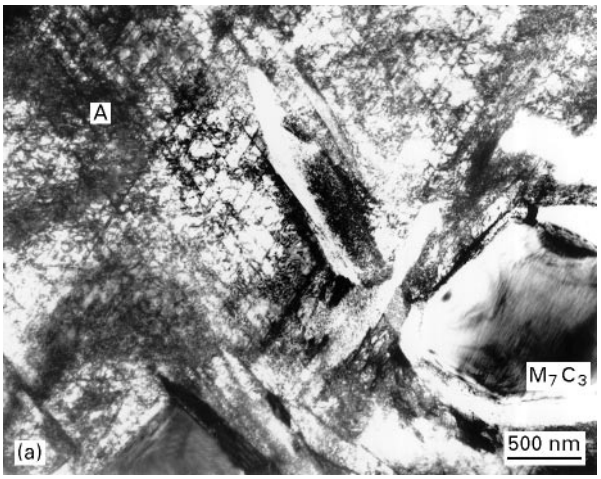

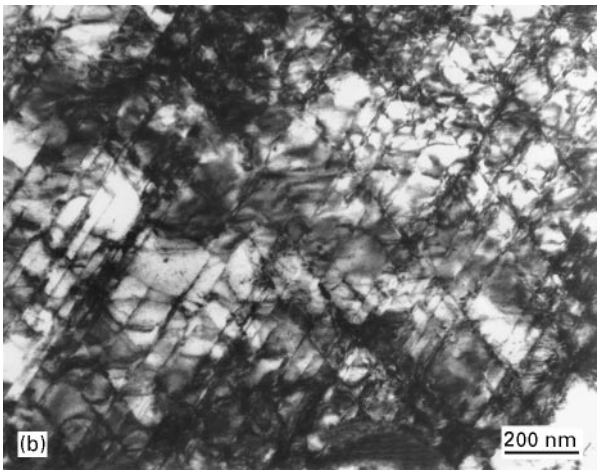

Figure 9 (a) and (b) Bright field images of the heat treated alloy showing contrast from the heavily faulted "bulk" retained austenite (A) in the dendritic microconstituent.

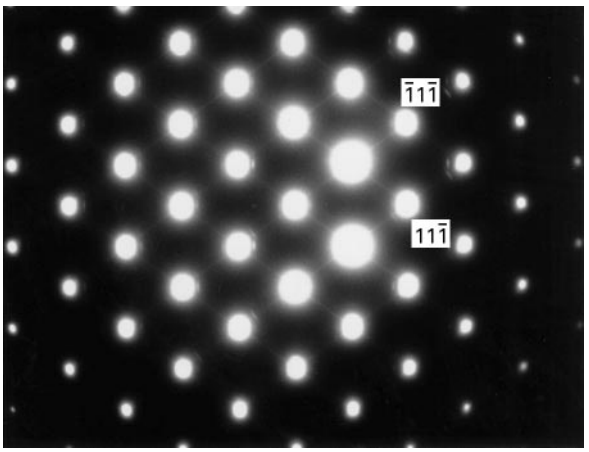

Figure 10 Electron diffraction pattern typical of those obtained from the heavily faulted 'bulk' retained austenite regions of the heat treated alloy. Pattern shows streaks corresponding to stacking faults on the close packed $\{1\,1\,1\}_\gamma$ planes. B = z = [0 1 1] face centred cubic (f c c).

happen unless there are secondary carbides to "entice" the crack out of the eutectic. It is possible that the SIM toughening mechanism is also dependent on this diversion of cracks into the dendrites.

The fracture behaviour in the toughened alloy is likely to be influenced by the precise distribution of

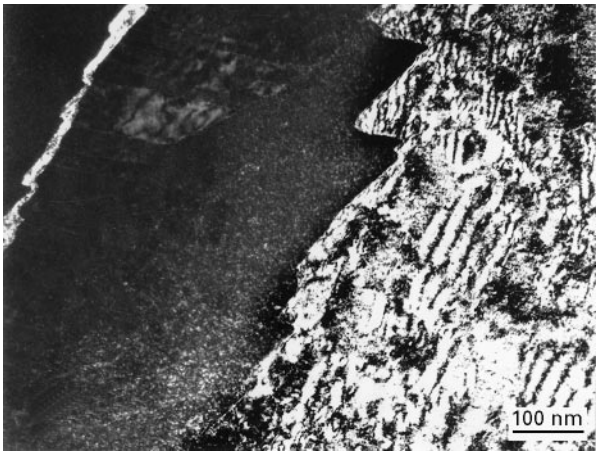

Figure 11 Dark field image of a region adjacent to a eutectic M_7C_3 carbide in the heat treated alloy. Contrast is visible from a morphology similar to that seen by Ricks *et al.* [25] in an Fe-Cr-Ni alloy which was identified as Widmanstätten ferrite sawteeth. In this case SAED was used to identify the illuminated phase as b c c iron.

martensite and retained austenite in the dendrites. This paper has shown that the secondary carbides are surrounded by sheaths of martensite, with laths extending into the remaining bulk austenite. It might be that these regions of martensite provide preferred paths by which cracks can travel from the eutectic to the secondary carbides. Once the crack has entered the interior of a dendrite, it is inevitable that some of the retained austenite in the vicinity of the advancing crack will experience strain. From the extent of the observed zone of transformation around the crack, one suspects that the strain field associated with the crack is sufficient to cause all metastable austenite for some distance ahead of the crack to transform. Thus the crack must be viewed as passing primarily through a matrix of martensite containing secondary carbides. On the other hand, XRD has shown that in the toughened alloy, even after either cryogenic treatment or gross deformation, the overall austenite to martensite ratio remains at approximately 0.35 (from 0.85 in the as-heat-treated condition) [9]. This represents a substantial fraction of stable retained austenite in the dendrites, thus there is a possibility that some crack energy might be absorbed in rupturing remaining ligaments of ductile stable austenite.

The bulk austenite in the heat treated alloy contains defect structures which have been shown by other authors to be associated with subsequent transformation to martensite. The M_s temperature of this austenite is around $-30\,^{\circ}C$, and it has been shown that this makes it accessible to strain-inducement of transformation. These defect structures are absent from the highly stable austenite of the as-cast alloy. It would be interesting to perform *in-situ* straining experiments in the TEM to observe the progress of transformation and, if possible, the paths of cracks through this constituent.

As stated above, even after cryogenic treatment or gross deformation there is a substantial volume fraction of stable retained austenite in the dendrites. The distribution of this phase may be of significance in the fracture behaviour. It would be difficult to obtain

thin-foil specimens from the deformed region around the crack, but information could be gained by examining foils from both bulk-deformed and cryogenically treated material. The morphology and distribution of the martensite formed by these two routes may be different, and these differences may provide clues to understanding the influence of transformation on fracture behaviour. The features of these two martensites could be further compared with those of the martensite formed naturally upon cooling of alloys destabilized at lower temperatures.

4. Conclusions

The microstructural features of the reduced-carbon alloy in the as-cast state have been found to be very similar to those of conventional high-carbon irons, with M_7C_3 eutectic carbides and stable retained austenite in the dendrites. The observation that the eutectic "matrix" is fully martensitic confirms earlier unsubstantiated beliefs.

The microstructural features of the heat treated alloy are again in many respects similar to those of more conventional 15–20 wt% Cr irons, with secondary carbides identified as M_7C_3. The dendritic matrix of this alloy, suggested by optical microscopy to be fully austenitic, has been found in fact to contain some martensite, and the possible effects of this on fracture behaviour have been discussed. The defect structures observed in the bulk retained austenite in the heat treated alloy are similar to those seen by other authors in stainless steels close to transformation, and it would be interesting to study their role in the transformation process.

In parallel with studies of the austenite from which transformation occurs, it would be desirable to investigate any morphological or distributional differences between martensites formed in the dendrites by different routes.

Acknowledgements

This work was performed with funding from the Australian Research Council. The authors wish to thank Dr. A. Kootsookos for provision of a copy of her PhD thesis.

References

1. D. E. DIESBURG and F. BORIK, in Proceedings of Symposium on Materials for the Mining Industry, Vail, Colorado, 1974, edited by R. Q. Barr (Climax Molybdenum Company) p. 15.
2. K. H. ZUM GAHR and W. G. SCHOLZ, *J. Metals* **32** (1980) 38.
3. K. H. ZUM GAHR and D. V. DOANE, *Metall. Trans. A* **11A** (1980) 613.
4. M. RADULOVIC, M. FISET, K. PEEV and M. TOMOVIC, *J. Mater. Sci.* **29** (1994) 5085.
5. F. MARATRAY and A. POULALION, *AFS Trans.* **90** (1982) 795.
6. G. L. F. POWELL and G. LAIRD II, *J. Mater. Sci.* **27** (1992) 29.
7. A. KOOTSOOKOS, PhD thesis, The University of Queensland, (1995).
8. A. KOOTSOOKOS, J. D. GATES and R. A. EATON, *Cast Metals* **7** (1995) 239.
9. S. K. HANN and J. D. GATES, *J. Mater. Sci.* **32** (1997) 1249.
10. P. DUPIN, J. SAVERNA and J. M. SCHISSLER, *AFS Trans.* **90** (1982) 711.
11. V. BISS, *Microstruct. Sci.* **7** (1979) 412.
12. J. T. H. PEARCE, *Wear* **89** (1983) 333.
13. *Idem*, *J. Mater. Sci. Lett.* **2** (1983) 428.
14. *Idem*, *AFS Trans.* **126** (1984) 599.
15. J. T. H. PEARCE and D. W. L. ELWELL, *J. Mater. Sci. Lett.* **5** (1986) 1063.
16. G. L. F. POWELL and J. V. BEE, *J. Mater. Sci.* **31** (1996) 707.
17. J. V. BEE, G. L. F. POWELL and B. BEDNARZ, *Scripta Metall. Mater.* **31** (1994) 1735.
18. W. DUDZINSKI, J. P. MORNIROLI and M. GANTOIS, *J. Mater. Sci.* **15** (1980) 1387.
19. J. P. MORNIROLI, E. BAUER-GROSSE and M. GANTOIS, *Phil. Mag. A* **48** (1983) 311.
20. T. OHIDE and G. OHIRA, *Brit. Foundryman* **76** (1983) 7.
21. P. R. HOWELL, J. V. BEE and R. W. K. HONEYCOMBE, *Metall. Trans. A* **10A** (1979) 1213.
22. R. W. K. HONEYCOMBE "Steels: microstructure and properties", (Edward Arnold Ltd, London, 1981).
23. J. W. BROOKS, M. H. LORETTO and R.E. SMALLMAN, *Acta Metall.* **27** (1979) 1829.
24. K. R. KINSMAN and J. C. SHYNE, *ibid.* **14** (1966) 1063.
25. R. A. RICKS, J. V. BEE and P. R. HOWELL, *Metall. Trans. A* **12A** (1981) 1587.

Received 19 April 1996
and accepted 28 January 1997